# Models of Single-Molecule Experiments with Periodic Perturbations Reveal Hidden Dynamics in RNA Folding

**Ying Li,[†,‡,§] Xiaohui Qu,[†,‡,§] Ao Ma,[#] Glenna J. Smith,[‡,§,⊥] Norbert F. Scherer,*[,‡,§,⊥] and Aaron R. Dinner*[,‡,§,⊥]**

*Department of Physics, James Franck Institute, Institute for Biophysical Dynamics, and Department of Chemistry, The University of Chicago, Chicago, Illinois 60637, and Department of Physiology and Biophysics, Albert Einstein College of Medicine, 1300 Morris Park Avenue, Bronx, New York 10461*

*Received: January 9, 2009; Revised Manuscript Received: April 2, 2009*

Traditionally, microscopic fluctuations of molecules have been probed by measuring responses of an ensemble to perturbations. Now, single-molecule experiments are capable of following fluctuations without introducing perturbations. However, dynamics not readily sampled at equilibrium should be accessible to nonequilibrium single-molecule measurements. In a recent study [Qu, X. et al. *Proc. Natl. Acad. Sci. U.S.A.* **2008**, *105*, 6602−6607], the efficiency of fluorescence resonance energy transfer (FRET) between probes on the L18 loop and 3′ terminus of the 260 nucleotide RNase P RNA from *Bacillus stearothermophilus* was found to exhibit complex kinetics that depended on the (periodically alternating) concentration of magnesium ions ($[Mg^{2+}]$) in solution. Specifically, this time series was found to exhibit a quasi-periodic response to a square-wave pattern of $[Mg^{2+}]$ changes. Because these experiments directly probe only one of the many degrees of freedom in the macromolecule, models are needed to interpret these data. We find that Hidden Markov Models are inadequate for describing the nonequilibrium dynamics, but they serve as starting points for the construction of models in which a discrete observable degree of freedom is coupled to a continuously evolving (hidden) variable. Consideration of several models of this general form indicates that the quasi-periodic response in the nonequilibrium experiments results from the switching (back and forth) in positions of the minima of the effective potential for the hidden variable. This switching drives oscillation of that variable and synchronizes the population to the changing $[Mg^{2+}]$. We set the models in the context of earlier theoretical and experimental studies and conclude that single-molecule experiments with periodic peturbations can indeed yield qualitatively new information beyond that obtained at equilibrium.

## 1. Introduction

Measurements of properties of individual molecules as time series (or "trajectories") are now enabling researchers to obtain information about the dynamics of conformational changes, binding events, and chemical reactions in a wide range of systems. Single-molecule trajectories have long been experimentally accessible in the case of the conductance of ion channels,[1,2] but similarly direct means of probing structural features have become available only in the past decade or so due to advances in optical detection.[3−6] In particular, intramolecular distances can now be probed by attaching dye molecules to sites of interest and measuring the efficiency of fluorescence resonance energy transfer (FRET).[3,5] This approach has been applied to monitor folding of biopolymers (proteins and nucleic acids),[7−9] enzyme−substrate complex formation,[10−14] and the operation of molecular motors.[15−20]

A persistent issue in such studies is that they explicitly follow the dynamics of one, or at most a few, of the many degrees of freedom of a macromolecular system. In other words, the measurement is a projection of the full dynamics. A macromolecular system typically has dynamics that span a range of time and length scales.[21,22] Because the FRET signal (coordinate) does not necessarily correspond to the slowest degrees of freedom (which may or may not coincide with those that best describe the reaction of interest), chemically identical molecules can appear to have a wide range of kinetics with differences persisting over long times.[23]

How best to interpret data in such situations remains an open question. One approach is to use a generalized Langevin equation (GLE) for the observable degree of freedom.[24,25] The dynamics of the remaining (hidden) degrees of freedom enter through a memory kernel and a random force that is correlated with itself over finite times (i.e., "colored noise"). An alternative means of generating complex kinetics is to postulate that the rates of the observable transitions depend on one or more fluctuating barriers that are assumed to be controlled by the hidden degrees of freedom.[26,27] While this mechanism is reasonable, such approaches have found limited application to date since, to the best of our knowledge, no systematic procedure for determining the statistics of the fluctuating barriers from data exists. Single-molecule data can often be assigned reliably to discrete states,[28,29] and Hidden Markov Models (HMMs) are quite popular owing to their ease of use in fitting such data.[30−33] In HMMs, one describes the kinetics with a set of discrete states connected by transitions with fixed exponential waiting-time distributions. The number of states can be larger than those observed to account for the hidden degrees of freedom and, in turn, the (complex) observed kinetics.

* To whom correspondence should be addressed. E-mail: nfschere@uchicago.edu (N.F.S.); dinner@uchicago.edu (A.R.D.).
† Department of Physics, The University of Chicago.
‡ James Franck Institute, The University of Chicago.
§ Institute for Biophysical Dynamics, The University of Chicago.
⊥ Department of Chemistry, The University of Chicago.
# Albert Einstein College of Medicine.

10.1021/jp900225q CCC: $40.75 
Published on Web 05/05/2009

Recently, Scherer and co-workers observed complex kinetics in single-molecule FRET studies of a large RNA molecule, the 260 nucleotide (nt) catalytic domain of the RNase P RNA from *Bacillus stearothermophilus* (termed $C_{thermo}$).[23,34] These studies examined the kinetics of interconversion within the collapsed state as a function of the concentration of magnesium ions in the solution (abbreviated as $[Mg^{2+}]$). RNA molecules equilibrated in a particular constant $[Mg^{2+}]$ condition fluctuate between two FRET states at low concentrations (0.01 and 0.1 mM) and several states at high concentrations ($\geq$1 mM).[23] The distributions of dwell times were fit well by biexponential functions at $[Mg^{2+}] \leq 0.1$ mM, suggesting that there are two channels for conformational change that differ with respect to the condition (or state of occupancy) of the hidden degree(s) of freedom.

In contrast to most single-molecule studies, Scherer and co-workers[34] also examined the dynamics in response to a driving force, a periodic change in $[Mg^{2+}]$. In these periodic perturbation experiments, $[Mg^{2+}]$ was varied in a square wave pattern with the concentration alternating between two levels, each persisting for a fixed time interval. Although the two FRET values (which we refer to as "states") visited were the same as those in the corresponding equilibrium cases at $[Mg^{2+}] = 0.01$ and 0.1 mM, the dynamics were strikingly different. Molecules in different FRET states (i.e., low and high) at the time of the $[Mg^{2+}]$ jumps exhibited different kinetics of relaxation and, in some cases, failed to reach their equilibrium FRET values at the end of the 10 s interval following each change in $[Mg^{2+}]$. Different molecules responded in a qualitatively different manner to the square-wave perturbation over time scales comparable to the duration of the experiment (minutes). These results suggest that the nonequilibrium experiments, at least to some extent, sample different regions of conformational space than do the equilibrium experiments. The availability of these data, with the contrast between the equilibrium and nonequilibrium behaviors, provides a unique opportunity to explore models for interpreting single-molecule data.

In this paper, we develop a hybrid continuous−discrete model to account for the dynamics of this RNA system in the two-state regime at low $[Mg^{2+}]$. In so doing, we show that the nonequilibrium measurements provide information beyond what is accessible at equilibrium. The observable degree of freedom is modeled as discrete with the two states connected by transitions with exponentially distributed waiting times. A variable that influences these rates and accounts for the remaining degrees of freedom evolves according to a Langevin dynamics in simple double-well potentials that depend on $[Mg^{2+}]$. The model captures the equilibrium behavior and, in contrast to purely discrete Markovian kinetic schemes, the nonequilibrium behavior. The relations to other approaches for interpreting single-molecule data are discussed.

## 2. Methods Section

**2.1. Single-Molecule $E_{FRET}$ Measurements.** Single-molecule experiments were performed by immobilization of biotinylated $C_{thermo}$ RNA on a 1% biotin−streptavidin-functionalized PEG coverslip[35] using a perfusion chamber gasket (SA50, Grace Bio-Laboratories), which allowed buffer exchange. Biotinylated PEG-functionalization and streptavidin binding were conducted according to published protocols.[5,35] $C_{thermo}$ was immobilized by 2 min of incubation with 50 pM RNA solution pre-equilibrated in the imaging buffer (20 mM Tris (pH 8) + desired $[Mg^{2+}]$). Cy3 and Cy5 dye molecules were attached specifically to the 3′ terminus and the L18 loop by hybridization (Figure 1). Fluorescence trajectories of surface-immobilized RNA were collected at room temperature (18 °C) in the presence of the glucose oxidase/catalase oxygen-scavenger system,[35] 0.8 mg/mL glucose oxidase, 0.03 mg/mL catalase, 1% $\beta$-mercaptoethanol, 0.4% glucose, and the desired $[Mg^{2+}]$. Single-molecule $E_{FRET}$ time trajectories with a 50 ms frame integration time were collected with an objective-type total internal reflection fluorescence (TIRF) microscope with an electron multiplying (EM) CCD array detector (iXon DV887-BI, Andor).[36]

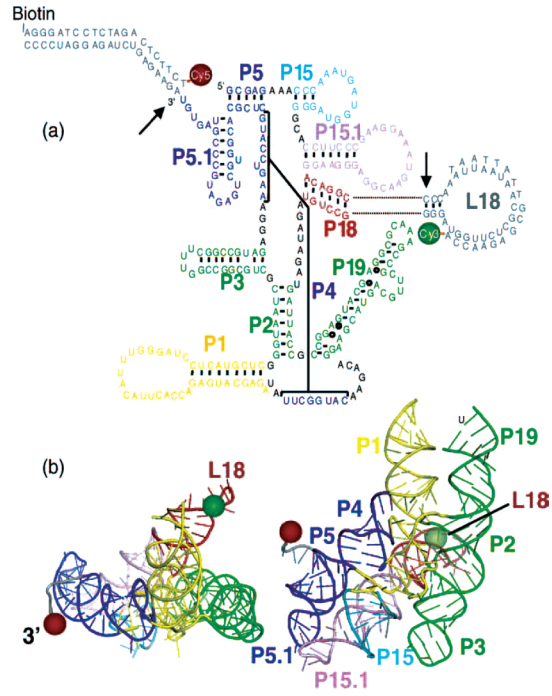


**Figure 1.** (a) Secondary structure representation for the catalytic domain of RNase P RNA from *Bacillus stearothermophilus* ($C_{thermo}$). (b) Approximate (three-dimensional) position of the Cy3 (green sphere) and Cy5 (red sphere) dyes, taken from ref 23 and based on the structure in ref 40.

**2.2. Hidden Markov Models.** In a Hidden Markov Model, the populations of different states evolve according to a discrete Master equation with fixed transition rates.[30,31] Detailed balance places constraints on the transition rates in the absence of a driving force. Given the initial state and transition probabilities, the probability of an observed sequence of states within a given model is a product of the probability of the initial state and the successive transition probabilities.

The transition rates were determined by maximizing the likelihoods of the experimental FRET trajectories with a Monte Carlo (MC) procedure.[37] To define the likelihoods, we grouped the states in the kinetic scheme into aggregated observable states ($n_i$, open or closed) and partitioned the transition rate matrix into corresponding blocks. Denoting the time the system jumped from state $n_{i-1}$ to $n_i$ by $\tau_i$, the probability of observing a particular sequence of observable states over total time $\tau$ ($\{n_i\};\{\tau_i\};\tau$) is

$$\mathscr{P}(\{n_i\};\{\tau_i\};\tau) = \vec{1}^{\mathrm{T}}\mathscr{G}_{n_k}(\tau_k,\tau)\mathscr{G}_{n_k n_{k-1}}(\tau_{k-1},\tau_k)\ldots\mathscr{G}_{n_2 n_1}(\tau_1,\tau_2)\mathscr{G}_{n_1 n_0}(0,\tau_1)\vec{\Theta}_{n_0}(0) \quad (1)$$

The vector $\vec{\Theta}_{n_0}(0)$ describes the initial probability distribution of all of the nonresolvable substates that belonged to the aggregated state $n_0$. $\vec{1}^{\mathrm{T}}$ is the transpose of a vector with all components equal to 1 that serves to sum over all possible final

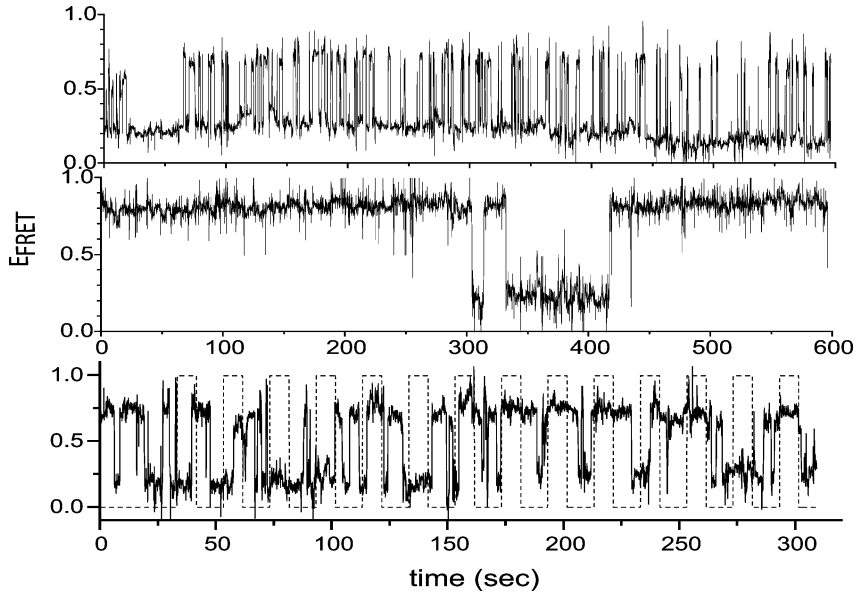


**Figure 2.** Representative single RNA $E_{FRET}$ trajectories. (top panel) Equilibrium experiment with low [$Mg^{2+}$] (0.01 mM). (middle panel) Equilibrium experiment with high [$Mg^{2+}$] (0.1 mM). (bottom panel) Nonequilibrium experiment with periodically changing [$Mg^{2+}$] between 0.01 and 0.1 mM; the idealized input [$Mg^{2+}$] profile is also shown (dashed line), although experimentally, it takes about 2 s for [$Mg^{2+}$] to switch from one value to the other.

substates. $\mathscr{G}_{n_i}(t_1,t_2)$ is the propagator for a process in which the system stays in state $n_i$ from time $t_1$ to time $t_2$ and remains there at the end of that time interval. $\mathscr{G}_{n_{i+1}n_i}(t_1,t_2)$ is the propagator for a process in which the system stays in state $n_i$ from time $t_1$ to $t_2$ and jumps to state $n_{i+1}$ at the end of that time interval. The propagators are formed from blocks of the transition rate matrix as detailed in ref 37.

The MC "energy" function ($E$) was the negative logarithm of the trajectory probabilities to avoid numerical overflow. Transition rates were initialized randomly from a uniform distribution ranging between $10^{-6}$ and 200 $s^{-1}$. At each MC step, the algorithm changed either one rate with a likelihood of 0.3 or all rates with a likelihood of 0.7. The new rates were obtained by multiplying the old rates by a random number $r_1$; $r_1$ had a power law distribution, $P(r_1) = 0.5/r_1$, and was restricted to the range $-1 \leq \ln r_1 \leq 1$. Moves were accepted when the energy change $\Delta E$ satisfied $\exp(-\Delta E/T) > r_2$, where $T = 0.001$ energy units is the MC "temperature" and $r_2$ is another random number uniformly distributed between 0 and 1. The parameters generally stopped evolving after 5000 MC steps (Figure 5). For the four-state HMMs, more than half of the 200 independent trials converged to a single set of parameters with the lowest energy accessed throughout the simulations (rates indicated in Figure 4A), which indicates that the data are sufficient to constrain the models.

**2.3. Generation of Trajectories with Periodic [$Mg^{2+}$] Changes.** In this section, we describe the methods used to simulate the nonequilibrium experiments, in which transition rates between discrete states are time-dependent. For the discrete degrees of freedom, we use a continuous-time Monte Carlo algorithm[38] modified to account for time-dependent reaction rates.[37] At each step of a simulation, a random number, $u$, is drawn from a uniform distribution over the interval (0,1], and the escape time $\tau_e$ is calculated by solving the equation $u = \exp[-\int_{\tau}^{\tau_e} a_{tot}(t)dt]$, where $\tau$ is the current time and $a_{tot}(t)$ is the sum of reaction propensities at time $t$. Once the time of the reaction is determined, the specific reaction executed is chosen with weights proportional to its propensity at that time, as in the unmodified algorithm.[38] In the experiments, the mixing time

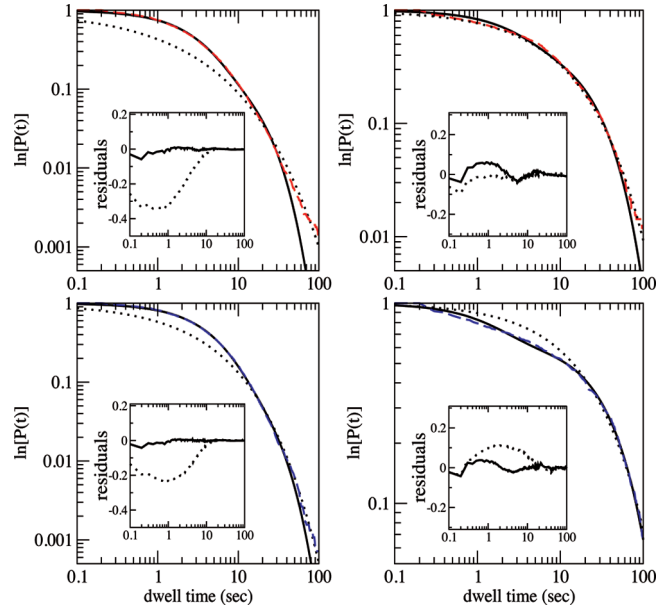


**Figure 3.** Accumulated dwell time distributions obtained from equilibrium experiments at [$Mg^{2+}$] = 0.01 (left panels) and 0.1 mM (right panels). The red dashed line is for low $E_{FRET}$ (open-to-closed transitions), and the blue dashed line is for high $E_{FRET}$ (closed-to-open transitions). Double exponential fits (solid black) and stretched exponential fits (black dotted) are also shown. Insets show residuals for the fits (same line types).

for [$Mg^{2+}$] to switch between 0.01 and 0.1 mM is nearly 2 s over the entire field of view but negligible at any given position. The effect of the average mixing time is thus to introduce some uncertainty into the actual period of the perturbation applied to any particular molecule. Here, we treat the change in the rates with [$Mg^{2+}$] as instantaneous, and we verified that our results are robust to small variations in the period (data not shown). We thus advance the time until either the next transition between substates (a "reaction") occurs or a transition rate changes with [$Mg^{2+}$]; $\Delta\tau = \min[-\ln u/a_{tot}(\tau), T_\tau - \tau]$, where $T_\tau$ is the next time when a rate changes. To obtain correct statistics in the latter case, the time is further advanced by $\Delta\tau' = -[\ln u +$

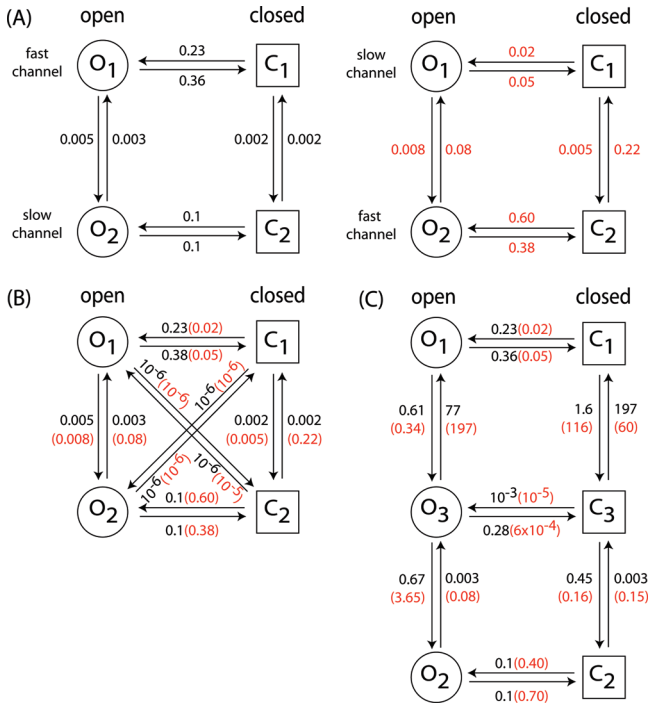


**Figure 4.** Four-state and six-state kinetic schemes constructed from HMM analysis. (A) Four-state scheme without cross connections; $[Mg^{2+}] = 0.01$ (left) and 0.1 mM (right). Molecules transitioning quickly (slowly) between open and closed FRET states at low $[Mg^{2+}]$ become the ones transitioning slowly (quickly) at high $[Mg^{2+}]$. As described in the text, we found empirically that the other mapping, in which molecules remain transitioning quickly (slowly) as $[Mg^{2+}]$ switches, fails to match the observed time scales of subensemble relaxation. The best fit rates in units of $sec^{-1}$ are as marked. (B) Four-state scheme with cross connections. (C) Six-state scheme. The rates shown are for one of the eight best fits. In parts (B) and (C), rates for $[Mg^{2+}] = 0.01$ mM are nonparenthetical, and those for $[Mg^{2+}] = 0.1$ mM are parenthetical (red).

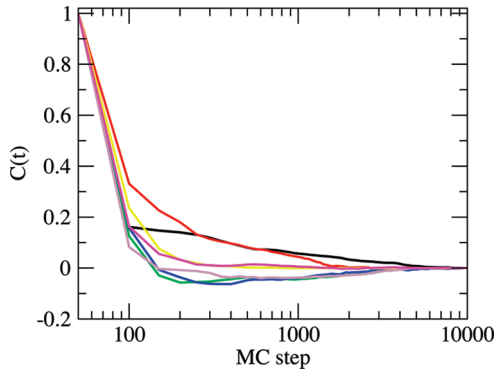


**Figure 5.** Convergence of the seven independent transition rates for low $[Mg^{2+}]$ in the scheme in Figure 4A. The correlation function $C(t)$ is defined as $[r(t) - r(\infty)]/[r(0) - r(\infty)]$, where $r(t)$ is the value of a rate constant at optimization step $t$. Simulations were stopped when 500 successive moves were rejected; all of the MC simulations were at least 10000 MC steps.

$a_{tot}(\tau)(T_\tau - \tau)]/a_{tot}(T_\tau)$. The algorithm described above is sufficient to integrate the HMMs forward in time, and we project the trajectories onto the observable states. For the hybrid model, reaction propensities $k_+$ and $k_-$ are determined by the hidden variable $X(t)$. The trajectories for $X$ were generated with a Verlet integrator using a time step of 0.005 s; the time-correlated random force was constructed using the procedure in ref 39.

## 3. Results

As discussed in the Methods Section, the experimental studies utilized the efficiency of energy transfer ($E_{FRET}$) between dye molecules on the L18 loop and 3′ terminus (Figure 1) to monitor structural dynamics of the 260 nt catalytic domain of RNase P from *B. subtilis*. The labeled regions are thought not to form tertiary interactions but to be sensitive to the structures of other parts of the ribozyme at all $Mg^{2+}$ concentrations studied.[40] Smith et al. proposed that conformational changes of specific structural units (P2, P4, P5 helices, and the L5.1-L15.1 and junction (J) tertiary interactions) are primarily responsible for the experimentally observed FRET dynamics.[23] In this section, we review the observations from these equilibrium experiments,[23] present new data obtained with a slightly modified protocol (see the Methods Section), and show that standard Hidden Markov Models (HMMs) can be used to fit these data. Subsequently, we present an analysis of the nonequilibrium data,[34] which necessitates a more complex model that can account for non-Poissonian dynamics. In particular, we develop a hybrid continuous−discrete model that captures the slow relaxation dynamics presumed to underlie the molecular heterogeneity discussed in the Introduction.

**3.1. Equilibrium Analysis.** Single RNA molecules were equilibrated in buffers, each of which had a particular $[Mg^{2+}]$. In the case defined as the low $[Mg^{2+}]$ regime (i.e., ≤0.1 mM), the $E_{FRET}$ fluctuated between two levels, $E_{FRET} = 0.2$ and 0.8. We refer to these $E_{FRET}$ values as "open" (i.e., extended) and "closed" (i.e., compact) states of the observed degree of freedom. In the high $[Mg^{2+}]$ regime (≥0.4 mM), $E_{FRET}$ populated a third value (0.45). In this paper, we focus on the apparent two-state kinetics at $[Mg^{2+}] = 0.01$ and 0.1 mM.

Inspection of individual trajectories shows that molecules behave in a persistent fashion; those that transition slowly continue to do so, while those that transition quickly continue to do so for essentially the full duration of trajectories (>10 min; Figure 2). Consistent with this observation, the dwell time distributions calculated from the $E_{FRET}$ trajectories of individual molecules are fit well by single exponentials at both $[Mg^{2+}]$ values, indicating simple (barrier crossing) kinetics for each molecule.[23] The microscopic transition rates vary from molecule to molecule, with no correlation between the rates of open-to-closed and closed-to-open transitions.

When the data for 250 molecules are pooled, the resulting dwell time distribution is well described by a biexponential function (Figure 3), which indicates the existence of two (or more) reaction channels connecting the open and closed states. A straightforward way to model the data is to construct a discrete kinetic scheme that includes states that are degenerate with respect to their $E_{FRET}$ values. Although transitions between these states are Markovian, the experimentally detectable kinetics are no longer Markovian because projection of the dynamics in the full space of the model onto $E_{FRET}$ introduces memory.[37]

Figure 4A shows the simplest kinetic scheme that can account for the biexponential dwell time distributions for both open-to-closed or closed-to-open transitions. It has four states with two intra-$E_{FRET}$-level connections and two inter-$E_{FRET}$-level connections. Each of the latter connections corresponds to an observable transition with an exponential waiting time distribution. We use a HMM approach as in refs 30 and 31 to obtain the transition rates (shown in Figure 4), including those for the hidden degrees of freedom that are not directly given by waiting time analysis. This approach seeks to find a set of parameters that maximizes the likelihood of the observed FRET trajectories given a model; it transcends the simple dwell time distribution

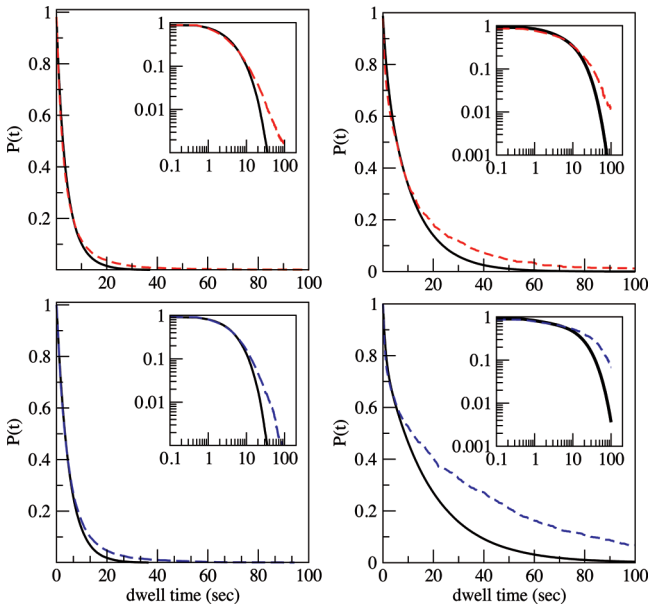


**Figure 6.** Accumulated dwell time distributions, $P(t)$. $[Mg^{2+}] = 0.01$ (left panels) and 0.1 mM (right panels). (top panels) Results from HMM simulations (black) and experiments (red dashed) for open-to-closed transitions. (bottom panels) Results from HMM simulations (black) and experiments (blue dashed) for closed-to-open transitions. Insets are the same results plotted on a log−log scale. The simulated trajectories are generated with the schemes in Figure 4A.

analysis by exploiting information about the sequence of consecutive transitions (see the Methods Section).

The dwell time distributions can be fit well by the resulting HMMs at times shorter than 10 s but not at times longer. Nevertheless, consistent with the observed persistence of individual molecular behaviors, the kinetics of the intra-$E_{FRET}$-level transitions are much slower than those of the inter-$E_{FRET}$-level ones. In other words, the vertical rates in Figure 4A (i.e., those governing the hidden degrees of freedom) are much smaller than the horizontal rates (i.e., those governing the observed degrees of freedom). Thus, the four-state HMM captures the behavior observed in the equilibrium experiments, at least qualitatively.

To test whether a kinetic scheme with more connections between microscopic states or more microscopic states would improve the match between the models and the experimental statistics, we applied the same HMM analysis to a four-state scheme with cross connections and a six-state scheme (Figure 4B and C). In the former case, the optimization procedure tended to decrease the rates for the cross connections until these transitions were negligible and the simpler four-state scheme was effectively recovered. For the six-state scheme, the fraction of independent runs that converged to the best fit was lower (8 out of 200 runs). The best fit is slightly poorer in quality than those obtained for the four-state schemes, and the rates, in particular, those for the intra-$E_{FRET}$-level transitions, vary to a much greater degree. Although there are three possible transition pathways between open and closed states (the horizontal connections in Figure 4C), the rates for the transitions between states $O_3$ and $C_3$ are such that the scheme effectively reduces to a four-state one again because the rates are such that molecules populating states $O_3$ and $C_3$ tend to transition vertically rather than horizontally in Figure 4C.

In summary, models of greater complexity than the simple four-state scheme in Figure 4A failed to improve the fit and reduced the level of confidence in the results. We thus take the simple four-state scheme to be the best HMM description of the equilibrium data.

**3.2. Nonequilibrium Analysis.** ***3.2.1. Review of Experimental Observations.*** Conceptually, a traditional nonequilibrium experiment would involve a single $[Mg^{2+}]$ jump and measurement of the relaxation of molecules to equilibrium. The kinetics obtained should be related to those in the aforementioned equilibrium studies through the fluctuation−dissipation theorem. Qu et al. employed an alternative perturbation method in which conformational fluctuations of an individual single molecule were explored in a nonequilibrium experiment as responses to a series of periodic $[Mg^{2+}]$ jumps.[34] Jumps between 0.01 mM (low $[Mg^{2+}]$) and either 0.1, 0.4, or 1.0 mM (high $[Mg^{2+}]$) were made with a period of 20 s. In the experiments with 0.1 mM as the high $[Mg^{2+}]$, molecules fluctuated between the $E_{FRET}$ levels observed at equilibrium. In contrast, in the experiments with 0.4 mM as the high $[Mg^{2+}]$, molecules populated more than the two $E_{FRET}$ states observed in the corresponding equilibrium experiments. Multiple $E_{FRET}$ levels were also observed in experiments with 1.0 mM as the high $[Mg^{2+}]$. As above, we restrict ourselves here to comparisons with experiments in which $[Mg^{2+}] = 0.01$ and 0.1 mM for simplicity. A typical trajectory from a nonequilibrium experiment jumping between these concentrations is shown in the bottom panel of Figure 2. Because the $[Mg^{2+}]$ period is shorter than the slowest relaxation times observed at equilibrium (i.e., hundreds of seconds for certain intra-$E_{FRET}$-level transitions in Figure 4A), we anticipate that the periodic perturbation would drive the system to conformations that are distinct from those sampled at equilibrium.

Qu et al. analyzed their data by partitioning it into subensembles that were defined by the two half-period intervals with a constant $[Mg^{2+}]$ and the $E_{FRET}$ levels at the initial time of each interval (i.e., high $[Mg^{2+}]$ starting with high $E_{FRET}$, high $[Mg^{2+}]$ starting with low $E_{FRET}$, low $[Mg^{2+}]$ starting with high $E_{FRET}$, and low $[Mg^{2+}]$ starting with low $E_{FRET}$).[34] For each subensemble, the fractions in the open and closed $E_{FRET}$ states were computed as a function of time within the period (Figure 7). This procedure revealed that equilibrium is not achieved in any of the four cases. More interestingly, RNA molecules with different initial $E_{FRET}$ values have different relaxation kinetics. In particular, the relaxation of the subensembles of molecules responding to a decrease in $[Mg^{2+}]$ exhibits a quasi-periodic response with a period of about 2.6 s. This pattern is also observed in analogous measurements with other $[Mg^{2+}]$ periods (from 10 to 40 s; unpublished data).

***3.2.2. Hidden Markov Model.*** In discrete-state Markov models of the form fit to the equilibrium data, the kinetics are determined by the eigenvalues of the rate matrices, and these eigenvalues must be negative real numbers to satisfy detailed balance under constant $[Mg^{2+}]$. The resulting (multi)exponential kinetics of population relaxation prevents such models (if kept sufficiently simple to fit the data confidently, see the discussion of ref 41 below) from giving rise to the quasi-periodic response described above (see Figure 7), despite the fact that we are driving the system in the nonequilibrium case through the periodic changes in $[Mg^{2+}]$. This assertion is supported by numerical results where trajectories were generated by toggling between the equilibrium kinetic schemes for $[Mg^{2+}] = 0.01$ and 0.1 mM in Figure 4A. In this regard, there is an ambiguity; the states $O_1$ and $C_1$ at low $[Mg^{2+}]$ could correspond to either the states $O_1$ and $C_1$ or the states $O_2$ and $C_2$ at high $[Mg^{2+}]$. In other words, it is not known a priori whether molecules transitioning quickly (slowly) between open and closed FRET states at low $[Mg^{2+}]$ remain the ones transitioning quickly

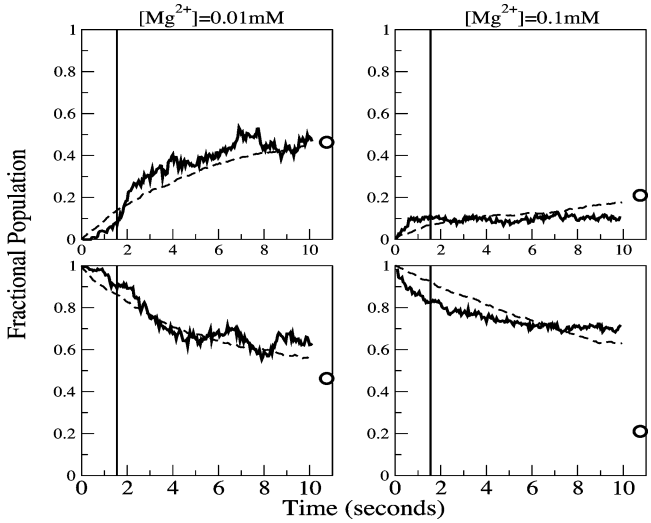


**Figure 7.** Subensemble analysis. Trajectories were grouped according to $[Mg^{2+}]$ (0.01 mM on the left and 0.1 mM on the right) and the initial FRET state in an interval (high FRET on the top and low FRET on the bottom), as described in the text. The fraction of the population in the low $E_{FRET}$ state is plotted. Circles correspond to the equilibrium distribution. The vertical lines at ≈2 s show when the $[Mg^{2+}]$ mixing period ends. Solid lines represent the experimental results; dashed lines represent the simulated results obtained by combining the four-state HMM schemes for low and high $[Mg^{2+}]$ in Figure 4A. Although it tends to somewhat underestimate the error, we can use bootstrapping to determine the statistical precision of the data; we randomly select events from the original data, calculate the subpopulation distribution for the selected data, and histogram the results for many trials. The width of each histogram is <1% for the two high $[Mg^{2+}]$ subensembles and <1.5% for the two low $[Mg^{2+}]$ subensembles.

(slowly) at high $[Mg^{2+}]$ or, instead, if they become the ones transitioning slowly (quickly). We thus explored both possible mappings between the two schemes in Figure 4A. The numerical procedure is described in the Methods Section. For simplicity, we assume molecules instantly adjust their kinetics with changes in $[Mg^{2+}]$. Partitioning the simulated trajectories into subensembles gives populations that relax with the same overall time scales as those observed in the experiments (dashed lines in Figure 7) when the fast (slow) channel at low $[Mg^{2+}]$ corresponds to the slow (fast) channel at high $[Mg^{2+}]$. No quasi-periodic response, however, is obtained in either mapping.

To ensure that the procedure above did not limit the ability to capture the quasi-periodic behavior, we also separately fit the nonequilibrium data with four-state kinetic schemes that are allowed to violate detailed balance (data not shown). If we assume that the transition rates change instantaneously with $[Mg^{2+}]$, there are 16 independent rates in total (8 for each $[Mg^{2+}]$). While the resulting discrete-state models capture the time scales of subensemble relaxation, they still do not give quasi-periodic responses. Indeed, the best-fit parameters between the open and closed states within a channel (fast or slow) are very similar to those obtained previously with the constraint.

Although this analysis is hardly exhaustive, we expect that an approach that allows for nonexponential relaxation kinetics is needed to capture the nonmonotonic population relaxation following a decrease in $[Mg^{2+}]$.

***3.2.3. Generalization of the Four-State Scheme to a Representation with Continuous Variables.*** Because the overall time scales of population relaxation are captured by the four-state schemes above, we build on them in constructing a model that describes the nonequilibrium observations. The HMM analysis suggests that description of the dynamics requires two variables, an observable one (corresponding to the horizontal transitions in Figure 4A) and a hidden one (corresponding to the vertical transitions). The hidden variable controls whether the observable variable is transitioning quickly or slowly. While one can go beyond exponential relaxation by postulating an arbitrary waiting time distribution or a memory kernel in a discrete-state model, a more transparent way is to let one of the degrees of freedom in the model vary continuously according to a simple Langevin dynamics in a potential.

Because we know that $E_{FRET}$ is well described by a discrete (two-state) variable, we modify the representation of the hidden variable. We specifically hypothesize that the quasi-periodic response in the subensemble analysis derives from intrabasin dynamics of the hidden variable. Denoting the hidden variable $X$, its equation of motion becomes

$$M\frac{d^2X(t)}{dt^2} = -\frac{dV(X(t);[Mg^{2+}])}{dX} - \gamma\frac{dX(t)}{dt} + f(t) \quad (2)$$

where $M$ is the mass of the hidden variable, $V(X(t);[Mg^{2+}])$ is the effective potential at a particular $[Mg^{2+}]$, and $\gamma$ is the friction coefficient. The stochastic force $f(t)$ is assumed to follow the usual fluctuation−dissipation relation $\langle f(t)f(t')\rangle = 2T\gamma\delta(t - t')$ with temperature $T$. The choice of $V$ is discussed in the following subsection.

The hidden variable influences the observable variable through the transition rates between open and closed states. In other words, the transition rates depend now on both $[Mg^{2+}]$ and the value of the hidden variable

$$\frac{dp_1(t)}{dt} = -k_+(X(t);[Mg^{2+}])p_1(t) + k_-(X(t);[Mg^{2+}])p_2(t)$$
$$\frac{dp_2(t)}{dt} = -k_-(X(t);[Mg^{2+}])p_2(t) + k_+(X(t);[Mg^{2+}])p_1(t) \quad (3)$$

where $p_1(t)$ ($p_2(t)$) is the likelihood for molecules to be open (closed) at time $t$ and $k_+(X(t);[Mg^{2+}])$ ($k_-(X(t);[Mg^{2+}])$) is the microscopic transition rate from open (closed) to closed (open). The dependence of $k_+$ and $k_-$ on the hidden variable is described following the form of the potential for the hidden variable. The idea of the model is that the hidden variable exhibits damped oscillations in response to the $[Mg^{2+}]$ driving; its dynamics influences the population of the open and closed states through its effects on the observable transition rates. The nonequilibrium periodic perturbation procedure serves to narrow the hidden variable positions accessed at the time of the changes in $[Mg^{2+}]$, and the subensemble analysis reveals this effective synchrony in the ensuing dynamics by partitioning trajectories according to the potential influencing the hidden variable and, through the initial FRET state, the transition rates available to the observable variable.

We work in units such that the mass of the hidden variable and the temperature are each 1. By construction, the hidden variable influences the observable variable but not vice versa. Physically, we imagine that the hidden variable represents a large part of the molecule and the observable variable represents a relatively small part of the molecule such that the effective inertia of the former is much larger than that of the latter. The hidden variable still fluctuates due to interactions with its environment; we choose a large friction for $[Mg^{2+}] = 0.1$ mM and a small friction for $[Mg^{2+}] = 0.01$ mM such that quasi-periodic responses are only observed in the relaxation profiles at low $[Mg^{2+}]$.

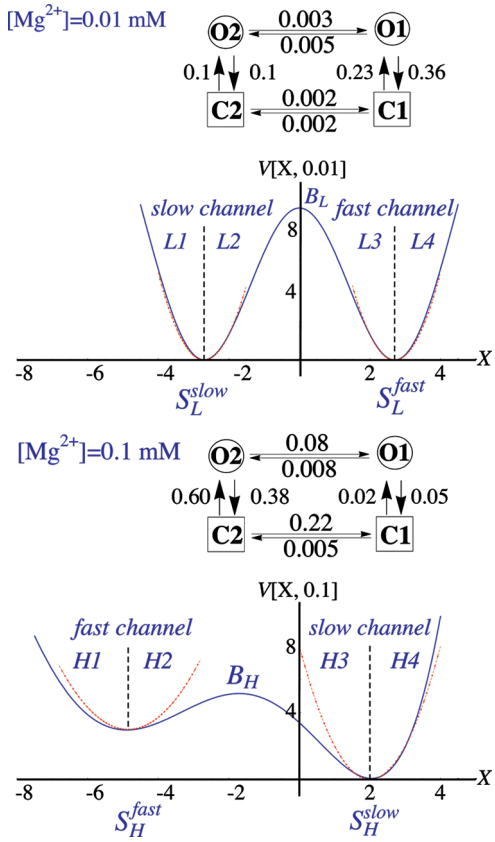


**Figure 8.** Hybrid model. Blue curves show the effective potentials for the hidden variable $X$ ($[Mg^{2+}] = 0.01$ mM on the top and $[Mg^{2+}] = 0.1$ mM on the bottom). Red dotted curves are harmonic approximations used to construct the potential wells. The wells are labeled as fast and slow, respectively, based on the relative sizes of resulting transition rates between open and closed observed states. The corresponding discrete-state models from Figure 4A are shown above the potentials. Parameters are given in Tables 1 and 2.

***3.2.4. Choice of the Hidden Variable Potentials.*** Given the general form of the model above, we need to specify the effective potentials in eq 2 that control the motion of the hidden variable. The simplest choice that would support oscillations of the hidden variable is a harmonic form (Figure 11A), but as discussed further below (section 3.2.7), this choice limits the ability of the model to capture the equilibrium dwell time distributions. The HMM analysis above indicates that the hidden variable has two stable states for each $[Mg^{2+}]$, which suggests that we should use a potential form with two wells in each case. To this end, we construct polynomials such that the minima are approximately harmonic (Figure 8)

$$V \approx V_i + \frac{1}{2}\omega_i^2(X - X_i)^2 \qquad \text{for} \quad X \approx X_i \tag{4}$$

where $V_i$, $\omega_i$, and $X_i$ are defined by eq 4 and $i$ labels stable states of the hidden variable, $S_L^{slow}$, $S_L^{fast}$, $S_H^{slow}$, and $S_H^{fast}$, with subscripts L and H for low and high $[Mg^{2+}]$, respectively, and superscripts slow and fast for slow and fast channels, respectively. These choices are made to ensure the correspondence between the HMM schemes in Figure 4A and the hybrid model as indicated by the discrete-state schemes shown in Figure 8.

With the aid of the earlier HMM analysis, we choose the parameters manually such that the model captures the nonequilibrium behavior qualitatively and the equilibrium behavior quantitatively. Values are given in Tables 1 and 2. We shift the positions of corresponding stable states at different $[Mg^{2+}]$ relative to each other such that sudden changes in $[Mg^{2+}]$ displace the hidden variable away from the potential minima and thus drive the system. In addition, we stipulate that the distance between stable states $S_L^{fast}$ and $S_H^{slow}$ be smaller than their respective distances to the barriers $B_L$ and $B_H$ (Figure 8) to ensure that the population is primarily confined to these two stable states, as revealed by the HMM analysis. In contrast, we require the stable state $S_L^{slow}$ be close to the barrier $B_H$ such that molecules tend to cross the barrier $B_H$ upon switching to the high $[Mg^{2+}]$ potential. We make the height of barrier $B_L$ higher than readily accessible by thermal fluctuations ($k_bT$, where $k_b$ is Boltzmann's constant) such that molecules transitioning slowly (rapidly) remain slow (fast) at constant low $[Mg^{2+}]$. We make the barrier $B_H$ somewhat lower since the HMM indicates that transitions of the hidden variable are a bit faster at high $[Mg^{2+}]$; we also introduce an asymmetry such that transitions from $S_H^{fast}$ to $S_H^{slow}$ are common (compare with Figure 4A in which the rates on the vertical transitions in the right-hand scheme tend to shift the population from the fast channel involving $O_2$ and $C_2$ to the slow channel involving $O_1$ and $C_1$). These many choices ensure that the overall kinetics of relaxation in both the equilibrium and nonequilibrium experiments are reproduced.

***3.2.5. Coupling between the Hidden and Observable Variables.*** We do not know how the hidden degree of freedom determines the transition rates of the observable one. For simplicity, we assume that $k_+$ changes abruptly as the hidden variable moves from one side to the other of each potential well (i.e., as $X$ crosses the dashed lines in Figure 8). The rates are based on the HMM results for the discrete four-state scheme (Figure 4A). That is, on average, transitions in the observed degree of freedom are fast when the hidden variable of the molecule is in one well (corresponding to the fast channel) but slow when the hidden variable is in the other well (corresponding to the slow channel). The rates are shown in Table 2.

***3.2.6. Numerical Results.*** We first compare results from our model with the equilibrium experimental measurements. At low $[Mg^{2+}]$, the waiting time distribution extracted from each trajectory is well fit by a single exponential function, but that obtained by pooling many trajectories requires a biexponential function. This observation is explained by the fact that thermal fluctuations at low $[Mg^{2+}]$ are not large enough for molecules to cross the barrier $B_L$. Therefore, only two types of trajectories in the hidden variable are observed (Figure 9 top panel). Each represents a molecule in which the hidden degree of freedom is confined to fluctuate within a basin ($S_L^{slow}$ or $S_L^{fast}$). At high $[Mg^{2+}]$, the waiting time distributions from single trajectories and the pool of many trajectories exhibit similar features to those at low $[Mg^{2+}]$. However, three types of trajectories in the hidden degree of freedom are observed (Figure 9 bottom panel): molecules fluctuating around the stable state $S_H^{slow}$ (black trajectory), molecules fluctuating around the stable state $S_H^{fast}$ (red trajectory), and transitions from $S_H^{fast}$ to $S_H^{slow}$ (green trajectory). Most of population is in the first category. The associated waiting time distributions are plotted in Figure 13.

We also simulate the nonequilibrium experiment with periodic changes in $[Mg^{2+}]$, as described in the Methods Section. Trajectories are segmented by the $[Mg^{2+}]$ jump transitions and grouped into subensembles in the same way as described earlier. The time courses of relaxation of the various populations are plotted in Figure 14. Consistent with the experiments, the subensemble with high $[Mg^{2+}]$ and low initial $E_{FRET}$ is far from equilibrium at the end of the interval. Relaxation in the low $[Mg^{2+}]$ intervals exhibits a quasi-periodic response with a frequency of 2.3 s, which is close to that measured experimentally.

**TABLE 1: Effective Potentials Governing Motion of the Hidden Variable ($V$ in eq 2 for the models in Figures 8, 11, and 12)[a]**

| $[Mg^{2+}]$ | model | $V(X; [Mg^{2+}])$ |
|---|---|---|
| 0.01 mM | Figure 8 (12) | $8.463 + 1.346 \times 10^{-2}X - 2.935X^2 - 4.113 \times 10^{-3}X^3 + 2.970 \times 10^{-1}X^4 + 2.971 \times 10^{-4}X^5 - 9.904 \times 10^{-3}X^6 - 5.896 \times 10^{-6}X^7 + 1.193 \times 10^{-4}X^8$ |
| | Figure 11A | $3.000(X + 3.000)^2$ |
| | Figure 11B | $1.316 \times 10 + 1.615 \times 10^{-2}X - 3.922X^2 - 4.936 \times 10^{-3}X^3 + 3.565 \times 10^{-1}X^4 + 3.565 \times 10^{-4}X^5 - 1.188 \times 10^{-2}X^6 - 7.075 \times 10^{-6}X^7 + 1.432 \times 10^{-4}X^8$ |
| 0.1 mM | Figure 8 (12) | $6.457 - 1.928X - 3.605 \times 10^{-1}X^2 + 1.643 \times 10^{-1}X^3 + 3.991 \times 10^{-2}X^4 + 7.408 \times 10^{-4}X^5 - 3.033 \times 10^{-4}X^6 - 2.267 \times 10^{-5}X^7 - 4.657 \times 10^{-7}X^8$ |
| | Figure 11A | $3.00000(X + 2.50000)^2$ |
| | Figure 11B | $1.618 - 3.400X + 1.051X^2 + 5.067 \times 10^{-1}X^3 - 2.024 \times 10^{-1}X^4 - 4.070 \times 10^{-2}X^5 + 1.306 \times 10^{-2}X^6 + 2.205 \times 10^{-3}X^7 - 2.827 \times 10^{-4}X^8 - 5.784 \times 10^{-5}X^9 + 9.563 \times 10^{-7}X^{10} + 5.649 \times 10^{-7}X^{11} + 2.476 \times 10^{-8}X^{12}$ |

[a] Additional parameters required for integrating the hidden variable equation of motion are the temperature for the Brownian motion ($T = 1$ energy unit), the mass ($M = 1$ mass unit), the friction coefficient at $[Mg^{2+}] = 0.01$ mM ($\gamma_l = 0.5$ mass unit $s^{-1}$), and the friction coefficient at $[Mg^{2+}] = 0.1$ mM ($\gamma_h = 10.0$ mass unit $s^{-1}$).

**TABLE 2: Rates of Transition for the Observed Degree of Freedom (for open-to-closed and closed-to-open transitions, $k_+$ and $k_-$, respectively, in eq 3) for the Models in Figures 8, 11, and 12**

| region | $k_+$ ($s^{-1}$) | $k_-$ ($s^{-1}$) | region | $k_+$ ($s^{-1}$) | $k_-$ ($s^{-1}$) |
|---|---|---|---|---|---|
| L1 | 0.05 | 0.10 | H1 | 0.46 | 0.60 |
| L2 | 0.13 | 0.10 | H2 | 0.26 | 0.60 |
| L3 | 0.20 | 0.23 | H3 | 0.07 | 0.02 |
| L4 | 0.50 | 0.23 | H4 | 0.03 | 0.02 |

The basis for the quasi-periodic response becomes obvious when we examine typical trajectories of the hidden variable (Figure 10). Molecules mostly populate stable states $S_L^{fast}$ and $S_H^{slow}$ (right basins in Figure 8) because those initially in the stable states $S_L^{slow}$ and $S_H^{fast}$ (left basins in Figure 8) cross the relatively low barrier $B_H$ during the high $[Mg^{2+}]$ intervals (the red trajectory in Figure 10) and do not return. The black trajectory in Figure 10 sketches how molecules respond to $[Mg^{2+}]$ changes. Molecules oscillate around $S_L^{fast}$ in the low $[Mg^{2+}]$ intervals and switch to the right shoulder of $S_H^{slow}$ when $[Mg^{2+}]$ increases. These molecules relax toward the minimum of $S_H^{slow}$ in the high $[Mg^{2+}]$ intervals, jump to the left shoulder of $S_L^{fast}$, and start oscillating again when $[Mg^{2+}]$ decreases. In this model, the changes in $[Mg^{2+}]$ kick molecules before they can dissipate their energy. Furthermore, relaxation toward a minimum prior to a switch in $[Mg^{2+}]$ narrows the distribution of positions of the hidden variable, and the driving thus acts to synchronize molecules.

The friction coefficient for the hidden variable is 10 mass units $s^{-1}$ at high $[Mg^{2+}]$ and 0.5 mass units $s^{-1}$ at low $[Mg^{2+}]$.

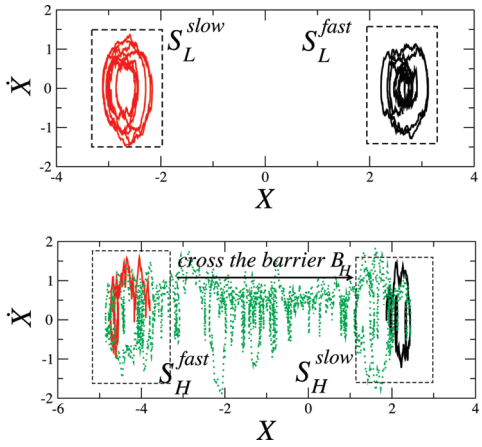


**Figure 9.** Equilibrium trajectories in the hidden degree of freedom for the scheme in Figure 8. (top panel) $[Mg^{2+}] = 0.01$ mM. Molecules are either in the fast (black) or the slow (red) channel. (bottom panel) $[Mg^{2+}] = 0.1$ mM. Molecules can stay in the slow channel (black) or the fast channel (red), or they can transition from the fast to the slow channel (green).

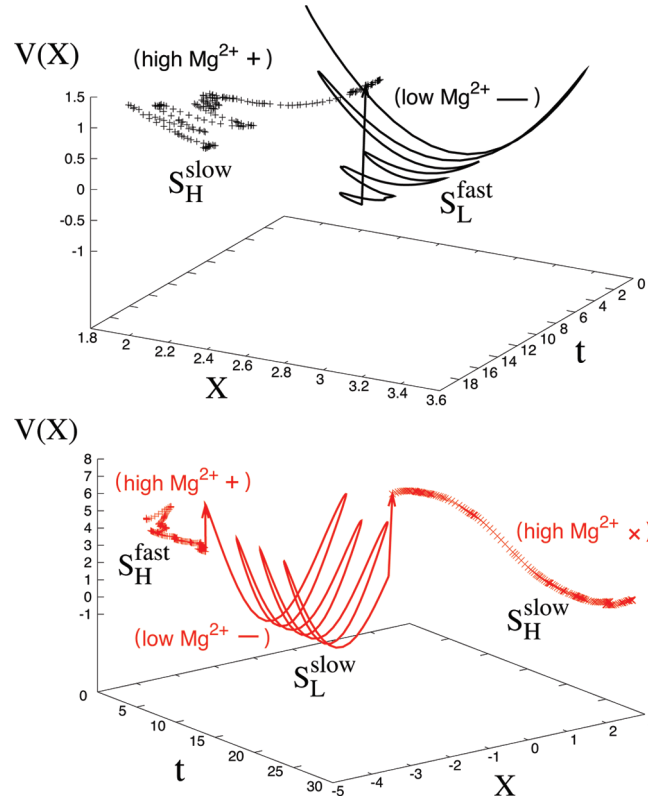


**Figure 10.** Nonequilibrium trajectories in the hidden degree of freedom for the scheme in Figure 8. $[Mg^{2+}]$ periodically changes between 0.01 and 0.1 mM. (top panel) A molecule oscillates in the stable state $S_L^{fast}$ during low $[Mg^{2+}]$ (black solid) and then moves toward the minimum of the stable state $S_H^{slow}$ during high $[Mg^{2+}]$ (black dashed). (bottom panel) A molecule in stable state $S_H^{fast}$ (red dashed) starts to oscillate around the stable state $S_L^{slow}$ with a large amplitude (red solid) following a decrease in $[Mg^{2+}]$. As $[Mg^{2+}]$ increases again, the molecule is able to reach the barrier $B_H$ and moves to the new stable state $S_H^{slow}$ (red dashed); it then follows a trajectory similar to the molecule depicted by the black curve in the top panel.

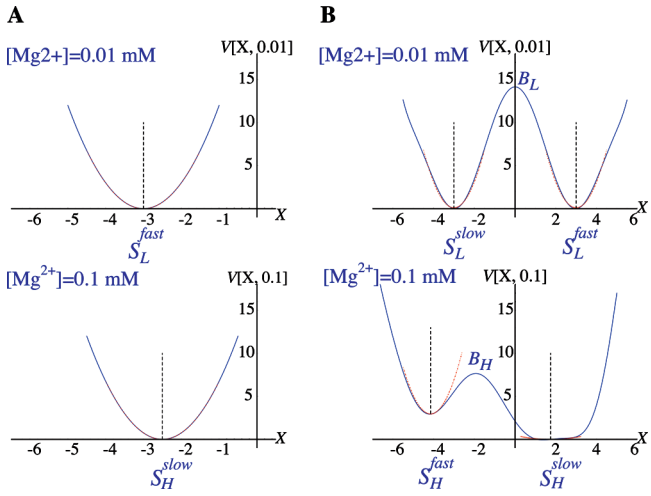


**Figure 11.** (A) Hybrid model with a single harmonic well for the hidden variable. (B) Hybrid model with an anharmonic stable state. Parameters are given in Tables 1 and 2.

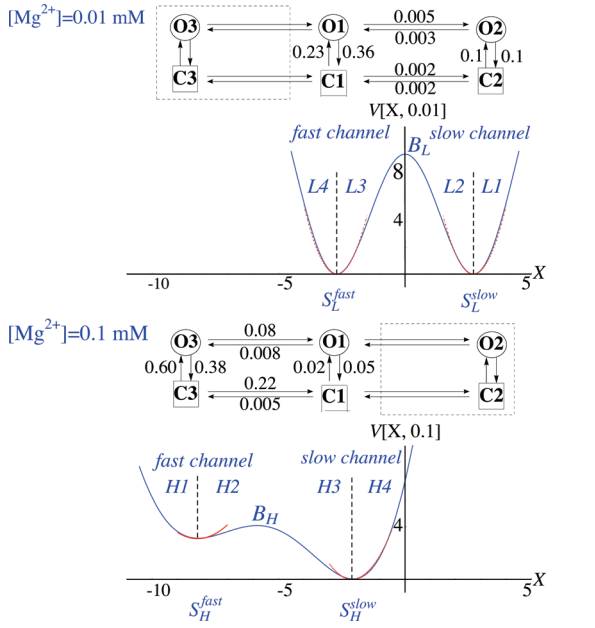


**Figure 12.** An alternative model that captures the observed behaviors. It differs from the model in Figure 8 with respect to the relative positions of the potentials wells. Parameters are the same as those in Figure 8 except that we swap the fast and slow channels for low [$Mg^{2+}$] and translate the effective potential for high [$Mg^{2+}$] to the left by 4.2 hidden variable units.

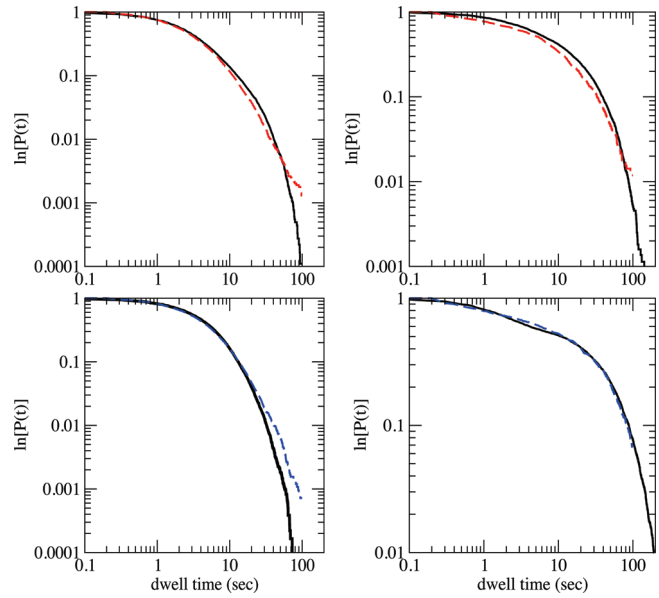


**Figure 13.** Accumulated dwell time distributions obtained with the hybrid model in Figure 8. The colors and panel arrangement are the same as those in Figure 6.

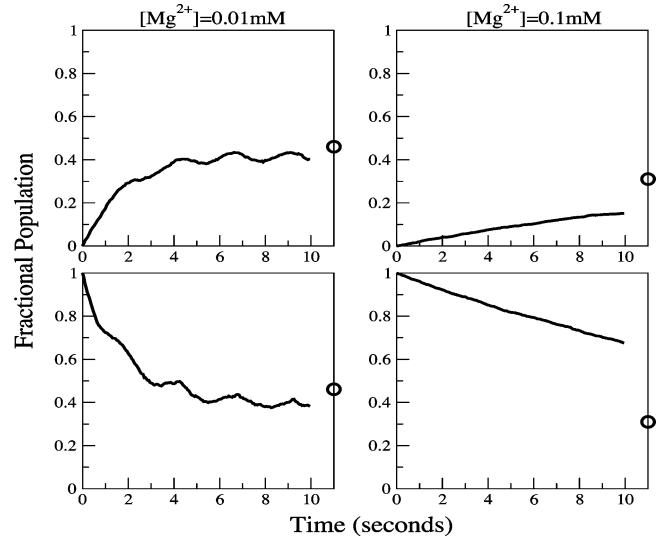


**Figure 14.** Subensemble analysis for trajectories generated from the scheme in Figure 8. The panel arrangement is the same as that in Figure 7. Again, the fraction of the population in the low $E_{FRET}$ state is plotted.

As in the experiments, there is no oscillation during the high [$Mg^{2+}$] intervals because the motion is overdamped; the decay rate of the oscillation amplitude $\gamma/2M$ is faster than the oscillation frequency $(\omega^2_{S_H^{slow}} - \gamma^2/4M^2)^{1/2}$, where $\omega_{S_H^{slow}}$ is the intrinsic frequency of the stable state $S_H^{slow}$. However, at low [$Mg^{2+}$], the hidden variable is underdamped. A parameter sensitivity analysis of the friction coefficient $\gamma$ establishes that the quasi-periodic behavior is still recognizable as long as the friction coefficient is no larger than 1.0 mass units $s^{-1}$ at low [$Mg^{2+}$]. While it is difficult to translate this figure to experimental units, owing to the fact that the identity of the hidden variable and, in turn, its effective mass are unknown, there is some precedence for apparently underdamped motions in nonequilibrium experiments, as reviewed in the Discussion.

***3.2.7. Alternative Models.*** To determine the degree to which the model is determined by the data, it is of interest to consider whether there are alternative effective potentials for the hidden variable that can also lead to the observed equilibrium and nonequilibrium dynamics. As mentioned previously, the simplest choice that gives rise to quasi-periodic responses in the subensemble analysis is a combination of two harmonic potentials (Figure 11A). The mechanism is essentially the same as above; periodic changes in [$Mg^{2+}$] repeatedly displace the hidden variable from its potential minima and, in the process, synchronize the population. We reject this model, however, because it gives rise to constant-[$Mg^{2+}$] dwell time distributions that are well fit by single exponentials.

One model that does completely capture both the equilibrium and nonequilibrium observed behaviors is shown in Figure 12. It is quite similar in spirit to but different in detail from that described in the previous sections. Owing to a shift in the positions of the stable states relative to the model in Figure 8, molecules with $X$ values that are low in energy at only one

$[Mg^{2+}]$ (i.e., those in $S_L^{slow}$ and $S_H^{fast}$) are forced to the overlapping basins $S_L^{fast}$ and $S_H^{slow}$ when the ionic environment is switched. This model maps to a discrete kinetic scheme with six states (as indicated at the top of Figure 12), but only four states are visited at each $[Mg^{2+}]$. The available data are insufficient to distinguish between the models in Figure 8 and 12.

In the models in Figure 8, there is no quasi-periodic response at high $[Mg^{2+}]$, owing to the fact that the amplitude of oscillation decays faster than the period when the friction is high. One might suppose that the quasi-periodic response could instead be suppressed at high $[Mg^{2+}]$ by the period being long (i.e., $2\pi/(\omega^2_{S_H^{slow}} - \gamma^2/4M^2)^{1/2} \gg 2M/\gamma$). To test this idea, we consider the potentials in Figure 11B in which we widen one basin; we set the friction coefficient at low and high $[Mg^{2+}]$ to be the same, $\gamma = 0.5$. Despite the fact that the potential at low $[Mg^{2+}]$ is unchanged, no quasi-periodic responses are obtained at either $[Mg^{2+}]$. Examination of the motion of the hidden variable reveals that, although the trajectories of individual molecules exhibit oscillations at low $[Mg^{2+}]$, molecules are distributed over both sides of the $S_L^{fast}$ basin upon a decrease in $[Mg^{2+}]$. Thus, the periodic $[Mg^{2+}]$ changes fail to synchronize molecules, which in turn results in a heterogeneity of rates for the observable variable and the loss of quasi-periodic responses in the subensemble analysis.

***3.2.8. Summary of Features of a Successful Hybrid Model.*** Although our exploration of models is not exhaustive, we believe the following features are required for the hybrid continuous−discrete framework considered here to capture the observed behaviors. We refer the reader to Figure 8 for an illustration of each point.

(1) The hidden variable must have two stable states. The barriers separating the stable states must be significantly higher than thermal fluctuations with that at $[Mg^{2+}] = 0.01$ mM somewhat higher than that at $[Mg^{2+}] = 0.1$ mM. These features are included to capture the characteristics of the equilibrium time series; molecules switch between open and closed states either rapidly or slowly in a persistent fashion.

(2) The distance between $S_L^{slow}$ and $S_H^{fast}$ must be sufficiently large that molecules are driven to oscillate around $S_L^{slow}$ with an amplitude that enables readily crossing $B_H$ upon switching to high $[Mg^{2+}]$. At the same time, the distance between $S_L^{fast}$ and $S_H^{slow}$ should be sufficiently small that molecules do not recross significantly to $S_L^{slow}$ and $S_H^{fast}$.

(3) The stable state $S_L^{fast}$ must be approximately harmonic to enable the hidden variable to oscillate at low $[Mg^{2+}]$. The stable states at high $[Mg^{2+}]$ ($S_H^{slow}$ and $S_H^{fast}$) can be nonharmonic, but their curvatures should be significantly larger than zero to enable synchronization of the population (contrast Figure 8 with 11B). The form of the stable states and their relative positions (with minima offset from each other) together determine the main nonequilibrium characteristics, quasi-periodic responses and failure to reach equilibrium within each interval of constant $[Mg^{2+}]$.

(4) The friction in the hidden degree of freedom must be low for $[Mg^{2+}] = 0.01$ mM (underdamped) and high for $[Mg^{2+}] = 0.1$ mM (overdamped).

(5) The rates of the observable transitions depend monotonically on the position of the hidden variable.

To satisfy items 1−3 above, we choose the frequencies for the stable states at low $[Mg^{2+}]$ ($S_L^{slow}$ and $S_L^{fast}$) to be larger than those for the stable states at high $[Mg^{2+}]$ ($S_H^{slow}$ and $S_H^{fast}$), so that $B_H$ is lower than $B_L$, but at the same time, the stable states are shifted appropriately relative to each other.

## 4. Discussion

In the present study, we have explored a series of models for the conformational dynamics of a large RNA molecule in different solution environments. In all of the cases considered, we limit the observable degree of freedom to discrete values and make the transition rates between states depend on another (hidden) degree of freedom. The hidden variable evolves continuously, and its synchronization and oscillation within a basin in response to changes in $[Mg^{2+}]$ are the basis for the striking relaxation kinetics revealed by partitioning molecules into subensembles. The essential features for reproducing the observed equilibrium and nonequilibrium behaviors within this theoretical framework are reviewed in the previous section.

Due to their prevalent usage, we initially applied a Hidden Markov Model (HMM) analysis to the RNA data. The HMMs that we employed were capable of capturing the equilibrium dwell time distributions to a certain degree, and they informed the choice of rates in the hybrid model that we constructed. The two stable states in the hybrid model correspond to the two channels (fast and slow) in the four-state kinetic scheme. HMMs were, however, completely inadequate for describing the nonequilibrium data. In this system, intrabasin dynamics of one degree of freedom are on the same time scale as interbasin dynamics of another. This feature cannot be described without resolving the intrabasin dynamics, and we thus expect other approaches based on only relaxation between discrete states[42] to fail similarly. Vlad and Ross suggest that the apparent violations in detailed balance needed to support oscillations in (cyclic) discrete kinetic schemes can be obtained if they arise from integration over intrastate fluctuations of a more complicated model,[41] but it is not clear what are the specific requirements on the original dynamics for this to be the case or whether typical data would be sufficient to constrain such a model.

We have also been able to describe the data qualitatively with a model based on the generalized Langevin equation (GLE) approach.[43] In that case, the observable degree of freedom evolved continuously in a double-well potential. Changes in $[Mg^{2+}]$ shift the well depths and drive molecules to cross the barrier, but the memory term in the equation of motion then causes a fraction to return at low $[Mg^{2+}]$. The picture is different in that the underdamped, quasi-harmonic component of the model is in the observable degree of freedom, with the equivalent of the hidden variable acting to restrain the observable one. However, the fundamental idea that there are two effective degrees of freedom with one acting in an underdamped, quasi-harmonic fashion is qualitatively the same. We have focused on the hybrid continuous−discrete model here because the dynamics of the hidden variable are more explicit (i.e., the path-dependent memory term can be difficult to interpret) and estimating the memory kernels needed for the GLE from limited data is not straightforward. It would be of interest in the future to solidify the connection between the present picture and a generalized Langevin or Master equation approach by integrating over the hidden variable to obtain an analytic form for the projected dynamics. Recent work on generating function approaches for systems with time-dependent Hamiltonians could be useful in this regard.[44]

The models considered here and in ref 43 can be viewed as explicit realizations of the general scheme outlined in ref 41, which relates the observed statistics (specifically, the fluorescence intensity correlation function) to intramolecular fluctuations by assuming temporally inhomogeneous dynamics. The transition rates between chemical states are random functions of time, and their stochastic

properties depend on a set of control variables that represent the fluctuations in the system configuration and, in turn, energy. Analytical results were obtained by further assuming a separation condition; that is, each transition rate was factorized into a universal component that depended on the control variables and was the same for all transitions and a process-dependent factor that depends on the initial and final state of the transition but not the time. Vlad and Ross[41] explicitly showed that quasi-periodic behavior can be obtained in the fluorescence intensity correlation function for an example similar to our model; the intramolecular fluctuations obey damped oscillatory dynamics (modes with complex eigenvalues) with characteristic time scales comparable to or longer than those of the transitions between observed states. However, that model[41] predicts damped quasi-periodic behavior in the correlation function even at equilibrium, which was not observed in our experiments. It could be that averaging over many molecules (with no way to "synchronize" their fluctuations) obscures these dynamics, while trajectories of individual molecules do not provide sufficient statistics. The nonequilibrium experiments and subensemble analysis overcome this problem by effectively synchronizing the intramolecular dynamics of many molecules to yield damped quasi-periodic responses in the relaxation profiles.

How underdamped modes would arise in the macromolecular system studied is not clear. Inelastic scattering measurements of proteins at equilibrium suggest that the slowest underdamped modes have motions on the picosecond time scale. However, the RNA molecule studied here is not at equilibrium. Regular oscillations with periods in the milliseconds have been reported for a mutant of green fluorescent protein (GFP) unfolding and refolding, and these can be extended to tens of milliseconds in resonant driving fields.[45] Certainly, the nature of the microscopic response of the molecule to $Mg^{2+}$ ions in its environment is not known with any detail and could contribute to the dynamics. In addition to the changes in $[Mg^{2+}]$ considered explicitly here, experimentally, the shear from the flow of buffer in the microfluidic channel on the (surface-tethered) molecule could result in a very slow apparent underdamped mode.[46] To assess this possibility, we are presently exploiting recent advances in simulating systems far from equilibrium[47,48] to investigate whether such cyclic motion exists in a simple polymeric model of this RNA[49] (A. Dickson, M. Maienschein-Cline, and A. R. Dinner, unpublished).

By eliminating the inhomogenous broadening among molecules, our technique makes it possible to display the dynamical information of fluctuations, in the spirit of photon echo experiments.[50] The subensemble behavior is different from the "event echo" proposed previously for quantifying the differences in parallel pathways between observed states.[51] The possibility of eliciting quasi-periodic respones in selected statistics (i.e., correlation functions) of observables in nonequilibrium single-molecule experiments suggests that mechanical and chemical analogues of NMR[52] can be developed. Such a spectroscopy would have profound consequences as it would enable one to study dynamics on relatively long (biologically relevant) time scales in systems that are not, in general, magnetically or optically active. Microfluidics now enable the straightforward generation of chemical pulse sequences,[34,53,54] but a theoretical framework is needed to design experiments rationally and maximize the information that can be extracted. The present study is a first step toward that goal.

**Acknowledgment.** This work was supported by the University of Chicago NSF-sponsored MRSEC (DMR0820054), the National Institutes of Health (GM067961), the Burroughs Wellcome Fund Interfaces ID 1001774 Fellowship (X.Q.), and a John S. Guggenheim Memorial Foundation Fellowship (N.F.S.).

## References and Notes

(1) Neher, E.; Sakmann, B. *Nature* **1976**, *260*, 799–802.
(2) Colquhoun, D.; Hawkes, A. G. *Proc. R. Soc. London, Ser. B* **1981**, *230*, 15–52.
(3) Selvin, P. R. *Methods Enyzmol.* **1995**, *246*, 300–334.
(4) Weiss, S. *Science* **1999**, *283*, 1676–1683.
(5) Ha, T. *Methods* **2001**, *5*, 78–86.
(6) Neuman, K. C.; Block, S. M. *Rev. Sci. Instrum.* **2004**, *75*, 2787–2809.
(7) Zhuang, X. W.; Ha, T.; Kim, H. D.; Centner, T.; Labeit, S.; Chu, S. *Proc. Natl. Acad. Sci. U.S.A.* **2000**, *97*, 14242–14244.
(8) Kim, H. D.; Nienhaus, G. U.; Ha, T.; Orr, J. W.; Williamson, J. R.; Chu, S. *Proc. Natl. Acad. Sci. U.S.A.* **2002**, *99*, 4284–4289.
(9) McKinney, S. A.; Declais, A. C.; Lilley, D. M. J.; Ha, T. *Nat. Struct. Biol.* **2003**, *10*, 93–97.
(10) Wouters, F. S.; Bastiaens, P. I. H.; Wirtz, K. W. A.; Jovin, T. M. *EMBO J.* **1998**, *17*, 7179–7189.
(11) Hiller, D. A.; Fogg, J. M.; Martin, A. M.; Beechem, J. M.; Reich, N. O.; Perona, J. J. *Biochemistry* **2003**, *42*, 14375–14385.
(12) Rueda, D.; Bokinsky, G.; Rhodes, M. M.; Rust, M. J.; Zhuang, X. W.; Walter, N. G. *Proc. Natl. Acad. Sci. U.S.A.* **2004**, *101*, 10066–10071.
(13) Antikainen, N. M.; Smiley, R.; Benkovic, S. J.; Hammes, G. G. *Biochemistry* **2005**, *51*, 16835–16843.
(14) Liu, S. X.; Bokinsky, G.; Walter, N. G.; Zhuang, X. W. *Proc. Natl. Acad. Sci. U.S.A.* **2007**, *104*, 12634–12639.
(15) Lucius, A. L.; Wong, C. J.; Lohman, T. M. *J. Mol. Biol.* **2004**, *339*, 731–750.
(16) Zhang, Z. Q.; Spiering, M. M.; Trakselis, M. A.; Ishmael, F. T.; Xi, J.; Benkovic, S. J.; Hammes, G. G. *Proc. Natl. Acad. Sci. U.S.A.* **2005**, *102*, 3254–3259.
(17) Hickerson, R.; Majumdar, Z. K.; Baucom, A.; Clegg, R. M.; Noller, H. F. *J. Mol. Biol.* **2005**, *354*, 459–472.
(18) Lee, T. H.; Blanchard, S. C.; Kim, H. D.; Puglisi, J. D.; Chu, S. *Proc. Natl. Acad. Sci. U.S.A.* **2007**, *104*, 13661–13665.
(19) Mori, T.; Vale, R. D.; Tomishige, M. *Nature* **2007**, *450*, 750–754.
(20) Guillaud, L.; Wong, R.; Hirokawa, N. *Nat. Cell Biol.* **2008**, *10*, 19–U8.
(21) Bokinsky, G.; Zhuang, X. *Acc. Chem. Res.* **2005**, *38*, 566–573.
(22) Min, W.; English, B. P.; Luo, G. B.; Cherayil, B. J.; Kou, S. C.; Xie, X. S. *Acc. Chem. Res.* **2005**, *38*, 923–931.
(23) Smith, G. J.; Lee, K. T.; Qu, X.; Xie, Z.; Pesic, J.; Sosnick, T. R.; Pan, T.; Scherer, N. F. *J. Mol. Biol.* **2008**, *378*, 941–951.
(24) Zwanzig, R. *Phys. Rev.* **1961**, *124*, 983-.
(25) Min, W.; Luo, G.; Cherayil, B. J.; Kou, S.; Xie, X. S. *Phys. Rev. Lett.* **2005**, *94*, 198302.
(26) Zwanzig, R. *Acc. Chem. Res.* **1990**, *23*, 148–152.
(27) Brown, F. L. H. *Phys. Rev. Lett.* **2003**, *90*, 028302.
(28) Watkins, L. P.; Yang, H. *Biophys. J.* **2004**, *86*, 4015–4029.
(29) Watkins, L. P.; Yang, H. *J. Phys. Chem. B* **2005**, *109*, 617.
(30) Qin, F.; Auerbach, A.; Sachs, F. *Biophys. J.* **2000**, *79*, 1915–1927.
(31) Qin, F.; Auerbach, A.; Sachs, F. *Biophys. J.* **2000**, *79*, 1928–1944.
(32) Andrec, M.; Levy, R. M.; Talaga, D. S. *J. Phys. Chem. A* **2003**, *107*, 7454–7464.
(33) McKinney, S.; Hoo, C.; Ha, T. *Biophys. J.* **2006**, *91*, 1941–1951.
(34) Qu, X.; Smith, G. J.; Lee, K. T.; Sosnick, T. R.; Pan, T.; Scherer, N. F. *Proc. Natl. Acad. Sci. U.S.A.* **2008**, *105*, 6602–6607.
(35) Rasnik, I.; Myong, S.; Cheng, W.; Lohman, T. M.; Ha, T. *J. Mol. Biol.* **2004**, *336*, 395–408.
(36) Qu, X.; Wu, D.; Mets, L.; Scherer, N. F. *Proc. Natl. Acad. Sci. U.S.A.* **2004**, *101*, 11298–11303.
(37) Li, Y.; Zhao, T.; Bhimalapuram, P.; Dinner, A. R. *J. Chem. Phys.* **2008**, *128*, 074102.
(38) Gillespie, D. T. *J. Phys. Chem.* **1977**, *81*, 2340–2361.
(39) Berkowitz, M.; Morgan, J. D.; McCammon, J. A. *J. Chem. Phys.* **1983**, *78*, 3256–3261.
(40) Kazantsev, A.; Krivenko, A.; Harrington, D.; Holbrook, S.; Adams, P.; Pace, N. *Proc. Natl. Acad. Sci. U.S.A.* **2005**, *102*, 13392–13397.
(41) Vlad, M. O.; Moran, F.; Schneider, F. W.; Ross, J. *Proc. Natl. Acad. Sci. U.S.A.* **2002**, *99*, 12548–12555.
(42) Flomenbom, O.; Silbey, J. *Proc. Natl. Acad. Sci. U.S.A.* **2006**, *103*, 10907–10910.
(43) Qu, X. *Non-equilibrium Magnesium-Concentration Jump Studies of the Early Folding Pathways of $C_{thermoL18}$ RNA*. Thesis, The University of Chicago, Chicago, IL, 2007.
(44) Zheng, Y.; Brown, F. L. H. *Phys. Rev. Lett.* **2003**, *90*, 238305.

(45) Baldini, G.; Cannone, F.; Chirico, G. *Science* **2005**, *309*, 1096–1100.
(46) Delgado-Buscalioni, R. *Phys. Rev. Lett.* **2006**, *96*, 088303.
(47) Warmflash, A.; Bhimalapuram, P.; Dinner, A. R. *J. Chem. Phys.* **2007**, *127*, 154112.
(48) Dickson, A.; Warmflash, A.; Dinner, A. R. *J. Chem. Phys.* **2009**, *130*, 074104.
(49) Hyeon, C.; Thirumalai, D. *Biophys. J.* **2007**, *92*, 731–743.
(50) Mukamel, S. *Principles of Nonlinear Optical Spectroscopy*; Oxford University Press: Oxford, U.K., 1999.
(51) Cao, J. *Chem. Phys. Lett.* **2000**, *327*, 38–44.
(52) Ernst, R. R.; Bodenhausen, G.; Wokaun, A. *Principles of Nuclear Magnetic Resonance in One and Two Dimensions*; Oxford University Press: Oxford, U.K., 1987.
(53) Bennett, M. R.; Pang, W. L.; Ostroff, N. A.; Baumgartner, B. L.; Nayak, S.; Tsimring, L. S.; Hasty, J. *Nature* **2008**, *454*, 1119–1122.
(54) Chen, D.; Du, W.; Liu, Y.; Kuznetsov, A.; Mendez, F. E.; Philipson, L. H.; Ismagilov, R. F. *Proc. Natl. Acad. Sci. U.S.A.* **2008**, *105*, 16843–16848.

JP900225Q